Deliverable Number D1.4: Report of simulation-assisted monitoring strategies; WP1; lead beneficiary no 8 (UiT)

Sub-seabed CO_2 Storage: Impact on Marine Ecosystems

Report of simulation-assisted monitoring strategies

Deliverable number 1.4

Stefan Bünz[1], Jim White[2], Sandra Hurter[1]

[1] Department of Geology, University of Tromsø, Norway

[2] British Geological Survey, Nottingham, UK

Deliverable description: Report of simulation-assisted monitoring strategies for seabed and sub-seabed leakage detection

Content

Aim of this report 3
Acknowledgement 3
1. Introduction 4
2. 4D processing of high-resolution 3D P-Cable seismic data 5
2.1 4D seismic concepts 5
2.1.1 Repeatability 6
2.1.2 Predictability 7
2.2 4D processing and analysis at Snøhvit 7
2.3 4D processing and analysis at Vestnesa Ridge 13
2.3.1 Cross-correlation coefficients and time-shifts 15
2.3.2 Predictability between the two volumes 16
2.3.3 4D processing 17
2.4 Concluding remarks on the 4D seismic processing of P-Cable 3D seismic data 22
3 Testing leakage detection thresholds using high frequency p-cable seismic data 24
3.1 Introduction 24
3.2 Potential CO2 leakage 25
3.3 P-cable data 27
3.4 Methodology - Statistical analysis 28
3.5 Concluding remarks on the estimation of detection thresholds from P-Cable 3D seismicdata . 31
4 References 32

Aim of this report

This report summarizes the work on developing monitoring technologies for the shallow subsurface based on the P-Cable 3D seismic technology. This work included the development of a 4D processing sequence undertaken by the University of Tromsø, and the analysis of detection thresholds of CO_2 in the shallow subsurface using of this high-resolution 3D seismic data.

Acknowledgement

The research leading to these results has received funding from the European Union Seventh Framework Programme (FP7/2007-2013) under grant agreement n° 265847.

1. Introduction

The ECO2 project has employed and adapted new baseline and monitoring technology for the shallow overburden of a storage site to facilitate a better identification of potential leakage pathways, detection of leaking CO_2 and monitoring. One of the new key technologies is P-Cable high-resolution 3D seismics.

The P-Cable 3D high-resolution seismic system consists of a seismic cable towed perpendicular (cross cable) to the vessel's steaming direction. An array of multi-channel streamers is used to acquire many seismic lines simultaneously, thus covering a large area with close in-line spacing in a cost efficient way. The cross-cable is spread by two paravanes that due to their deflectors attempt to move away from the ship. The P-Cable system is designed and developed as a tool for marine geological research and the petroleum industry. It may be used in both frontier and mature regions in an intelligent, versatile way to acquire successive small-size surveys (25 to 250 km2) in areas of special interest, e.g. 4D seismic monitoring of the shallow overburden at CO_2 storage sites. This is due to the fast deployment and recovery of the P-Cable and the short turns needed between adjacent sailing lines. The P-Cable technology has proven data quality, surpassing conventional 3D and equal or better than HiRes 2D. The increase in lateral resolution compared to conventional 3D seismic data is approximately one order of magnitude. This technology images the top500-800 m of the overburden in high detail and ideally complements conventional 3D seismic data, which is the premier monitoring tool for CO_2 storage.

In the first part of this report, the initial 4D seismic processing sequence developed by the UiT will be presented and assessed using a number of available 4D seismic attributes. Based on the processed 4D seismic data, BGS estimates detection thresholds for small amounts of CO_2 that may be detected in the shallow overburden using the P-Cable technology.

2. 4D processing of high-resolution 3D P-Cable seismic data

This chapter presents the development and application of a 4D seismic processing and analysis workflow applied to P-Cable 3D seismic data with relatively high frequency and large bandwidth (30-350 Hz) compared to conventional 3D seismic data. The P-Cable system offers full 3D seismic data acquisition using parallel streamers with high resolution which makes it superior to any other method to image the upper few hundreds of meters beneath the seabed in unprecedented detail (Peterson, et al., 2010).

The P-cable system operates with 14 parallel streamers spaced every 12.5 m along the cross-cable. The cross cable curves during acquisition meaning the streamers are only offset by 10-12 m. Shots are fired every 4 seconds using a mini-Gi gun with a pressure of 170 bar.

The 4D processing was applied to repeat seismic data from the Snøhvit CO_2 storage site in the Barents Sea, one of the two major industry sites in the ECO2 project, and to 4D data from the Vestnesa Ridge off the western continental margin of Svalbard, where gas actively seeps from the seafloor. Each of the data sets used the same 4D seismic processing principles but used a different 4D seismic software package. For the Snøhvit data, we used Landmark's SeisSpace Promax4D package, and for the Vestnesa data we used CGG Hampson-Russel Pro4D.

2.1 4D seismic concepts

The concept of 4D seismic is to use repeated 3D seismic data over an area to monitor the changes in the subsurface. Changes in the subsurface due to fluid flow will change properties such as fluid saturation, temperature, porosity and pressure, and hence the elastic properties of the rock, which cause a change in seismic response (Johnson, 2013). Two or more seismic surveys are being repeated at different times, whereby the first survey is considered the base and all following surveys the monitors.

By applying a fourth dimension, time, to 3D seismic data we can observe subsurface changes due to fluid flow or depletion of a reservoir in production. 4D, time-lapse data, have now been used as a monitoring tool for more than 20 years mostly for CO_2 storage and enhanced oil recovery projects. By using qualitative 4D data one can gain knowledge about the complexity of a dynamic subsurface and reduce reservoir-model uncertainty.

The goal of 4D processing is to:

- Maximize repeatability
- Preserve and resolve differences in the data that occur due to fluid flow
- Preserve true relative amplitudes and arrival times (Johnson, 2013).

Interpretable 4D seismic relies highly on repeatability, a measure of the similarity of several seismic datasets. Repeatability can be characterized by two parameters, NRMS and predictability, that were calculated throughout the whole 4D processing.

2.1.1 Repeatability

As a time-lapse seismic survey aim is to compare two or more 3D seismic surveys at the same location, but at different times, it is important that the acquisition geometry is repeated as good as possible. Acquisition differences may hide the seismic response over time due to fluid flow/changes in the subsurface.

Repeatability is about producing two or more images over the same location with a time interval between. Several factors contribute to whether the repeatability of time-lapse data is good or not. The most important factor is repeatability of the acquisition, hence that the source-receiver equipment and geometry including acquisition direction remains the same during base and monitor survey. Only a small shift in position will alter the quality of the time-lapse data, difference in source receiver geometry imply different ray paths through the overburden and hence different illumination of target (Johnston, 2013). In most cases this is impossible. Several factors such as water currents, tidal, salinity, seasonal temperature changes, weather condition and topography makes it impossible to create a rerun of baseline acquisition during monitor acquisition (Oghenekohwo & Herrmann, 2013). Even though the acquisition repeatability is not obtained perfectly the repeatability of processing of the 3D data will, if done correctly, reduce noise and processing artifacts and enhance the time-lapse data.

Repeatability is often measured in NRMS. The lower the NRMS value is, the better the match between base and monitor is, hence the better repeatability. In acquiring the 3D data two main methods are being used, permanently installed seismic cables at the seabed (PRM) or by a towed streamer. Towed streamers normally achieve a NRMS above 20%, while PRM has shown to achieve lower than 5% (Eriksrud, 2014). It is important to notice that these values are taken from conventional 3D seismic data. In this case we will use relatively high frequency P-cable 3D seismic data acquired by towed streamers. The bandwidth of the P-Cable data is approximately 30-350 Hz.

The normalized root-mean-square (NRMS) is defined as the root-mean-square (RMS) of the difference between the two datasets divided by the average of the RMS of each dataset. Its value is expressed as a percentage ranging from 0% if the two datasets are identical to 200 % if they are completely different. NRMS is very sensitive to static, phase and amplitude differences.

$$NRMS = \frac{200 \times RMS_{monitor-base}}{RMS_{monitor} + RMS_{base}}$$

2.1.2 Predictability

Predictability is a measure of how closely two seismic volumes values follow each other, or how similar they are. A good match would be as close to 100%. Several of the factors mentioned in 2.1.1 contribute to whether two surveys are similar or not. In areas where there have been movement of fluid the predictability is often poor.

Predictability is defined as the sum of the squared cross-correlation divided by the sum of the product of the autocorrelations. It quantifies the likeness of the two datasets and is expressed as a percentage ranging from 0% if the two datasets are completely different to 100 % if they are identical.

$$\mathrm{PRED} = \frac{100 \times \sum \Phi_{ab}(\tau) \times \Phi_{ab}(\tau)}{\sum \Phi_{aa}(\tau) \times \Phi_{bb}(\tau)}$$

Predictability is calculated over a given time window in the seismic data. The predictability is more sensitive to noise and distortion than to time shift. So even if the time shift is big, the predictability can still be good. Big shifts in time can be produced by change in fluid concentration as these changes will decrease or increase the velocity of seismic waves, and hence cause pull-up or push down of reflections.

2.2 4D processing and analysis at Snøhvit

The workflow developed for the 4D processing of the two high-resolution 3D P-Cable seismic datasets acquired in 2011 and 2013 in the Snøhvit area is presented in Figure 1. This workflow was designed to match the two seismic data sets and potentially highlight the changes due to fluid migration and variation in the amount of (free-)gas, and to remove non-geologic differences and non-repeatable noise due to acquisition and/or 3D processing differences.

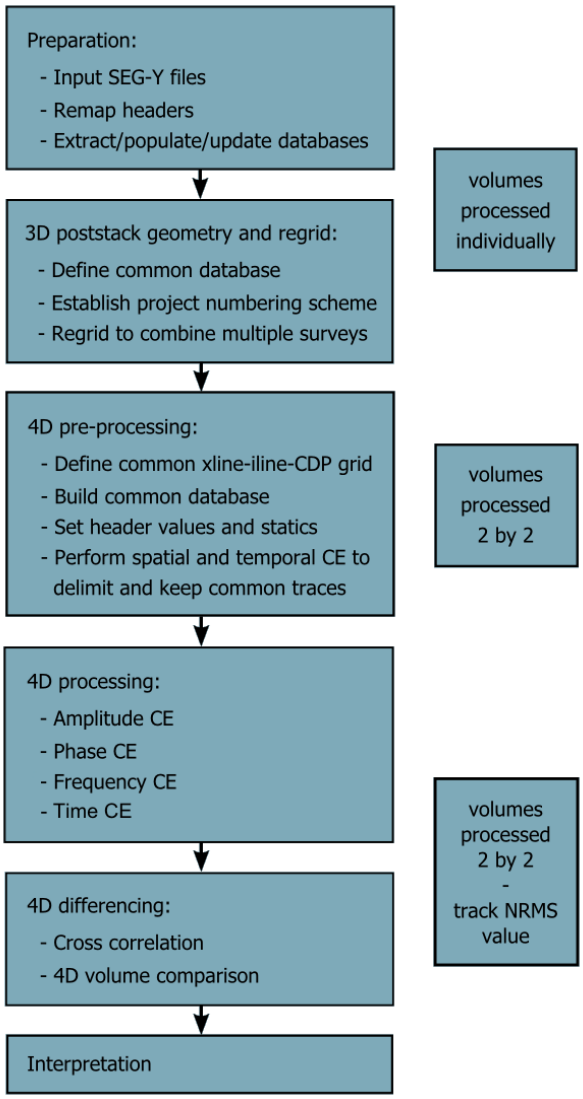

Figure1: 4D processing workflow

During the preparation phase, both 3D volumes were processed individually before the beginning of the 4D processing itself. Each SEG-Y files was imported into SeisSpace ProMAX® and databases were created and populated with values extracted from the trace headers (numbering scheme and geographic position). The orientation and design of the binning grid was checked for each volume as well.

The two datasets having different sizes, orientations and numbering schemes, a common scheme was established and the corresponding database was built. The 2013 dataset was regridded to match the 2011 dataset, and both datasets were renumbered consistently.

Spatial and temporal cross-equalization (CE) were performed during the 4D preprocessing phase to keep only traces that are in common in the two volumes. The corresponding shared database was updated to define the new common binning grid, reference coordinates, spatial extent and numbering scheme (Figures 2 and 3). The final outputs were also checked to

ensure that each line of the intersected volumes has the same number of CDP and dead traces due to the regridding were removed at the edges.

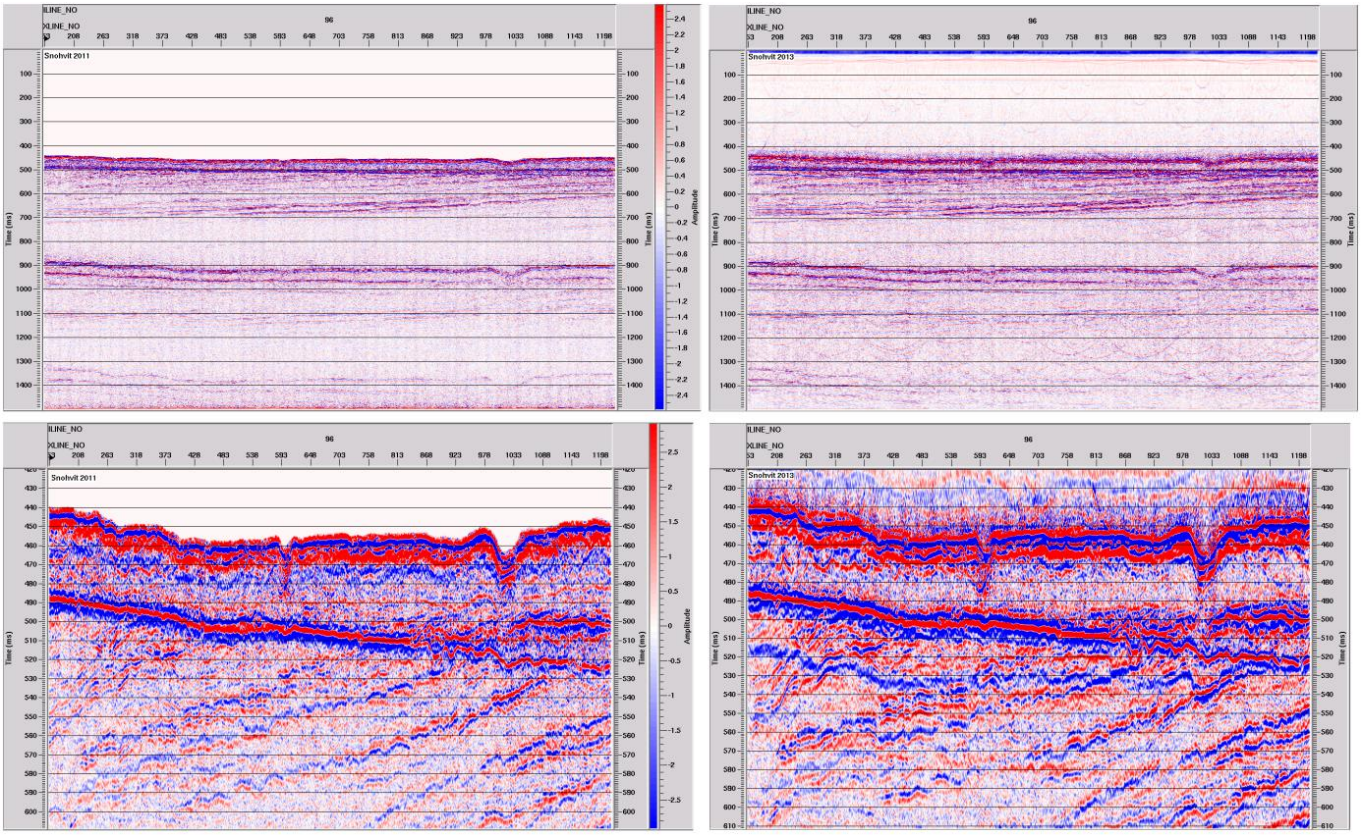

Figure 2 Snøhvit 2011 and 2013 datasets at the beginning of the 4D preprocessing.

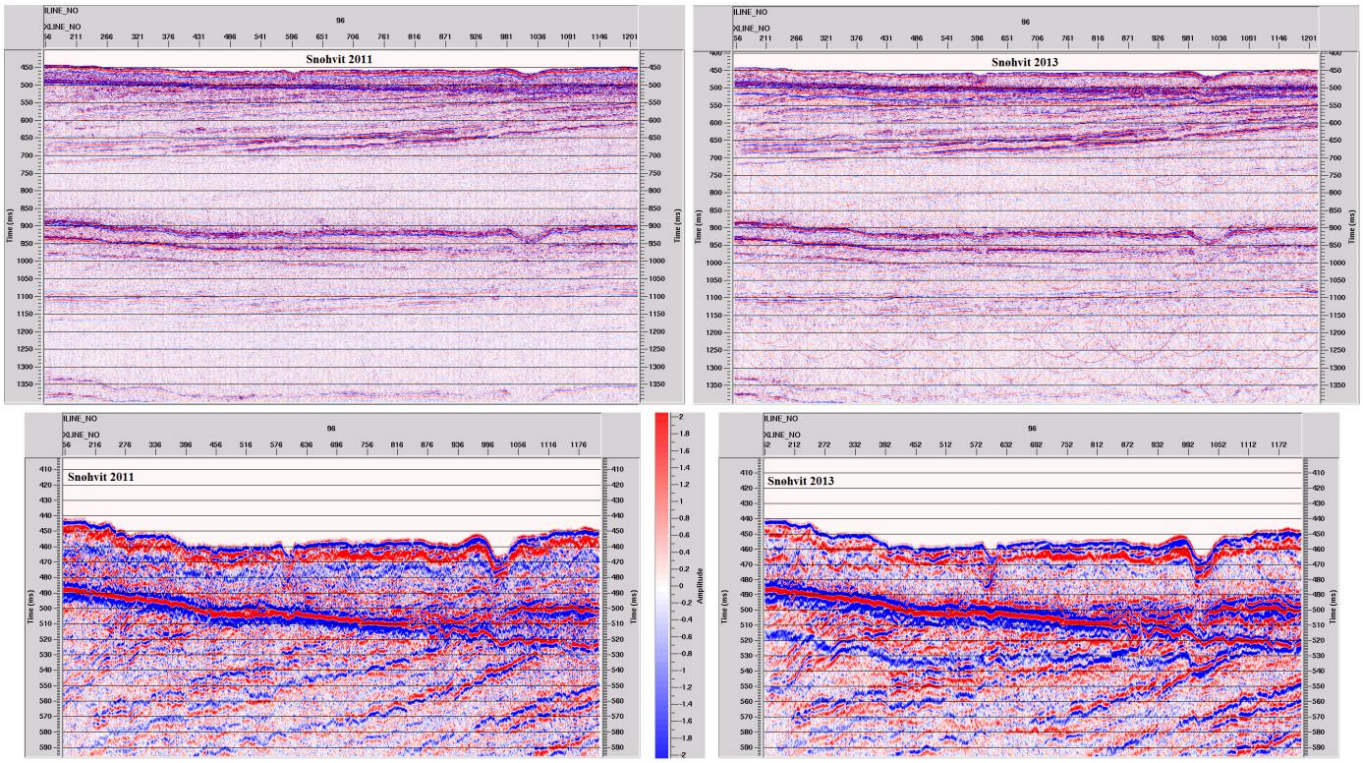

Figure 3: Snøhvit 2011 and 2013 datasets at the end of the 4D preprocessing.

The 4D processing stage aims at minimizing the difference in amplitude, time, phase and frequency content between the two volumes. The 2011 dataset was used as the control dataset.

Orienting and aligning surveys to remove structural differences is a key point, as well as identifying desirable data characteristics. Global inline, crossline, time and phase shifts were computed and applied to align the datasets (figure 4).

A frequency balance was applied to ensure that both datasets share a common amplitude spectrum before the amplitude cross-equalization was performed.

Cross-correlations and auto-correlations were generated and run to compute match filters before applying them. These filters force the phase and amplitude characteristics of the 2013 dataset to match those of the 2011 dataset (figure 5).

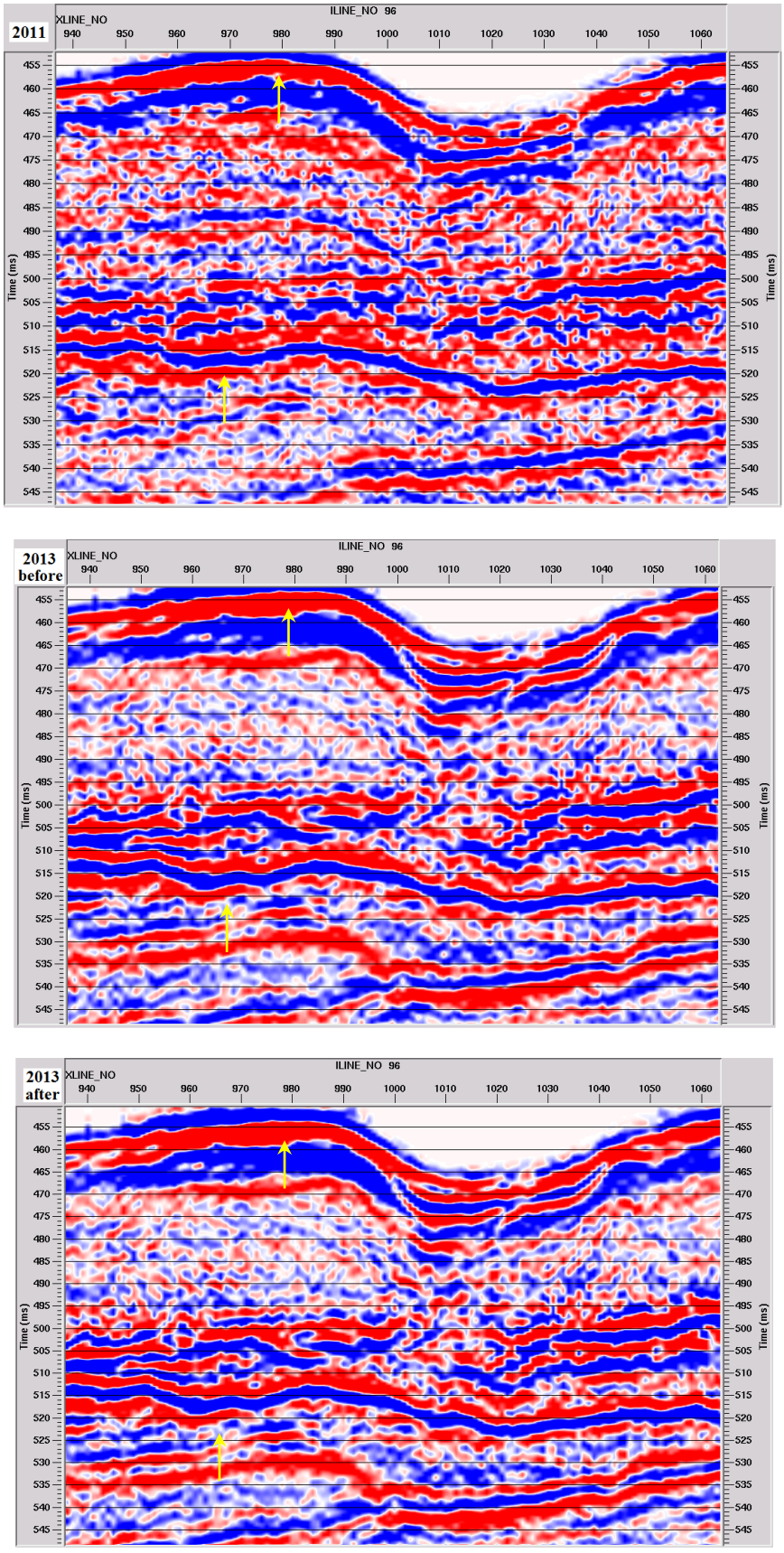

Figure 4: Global inline, crossline, time and phase shifts applied to the Snøhvit 2013 dataset to match the 2011 dataset.

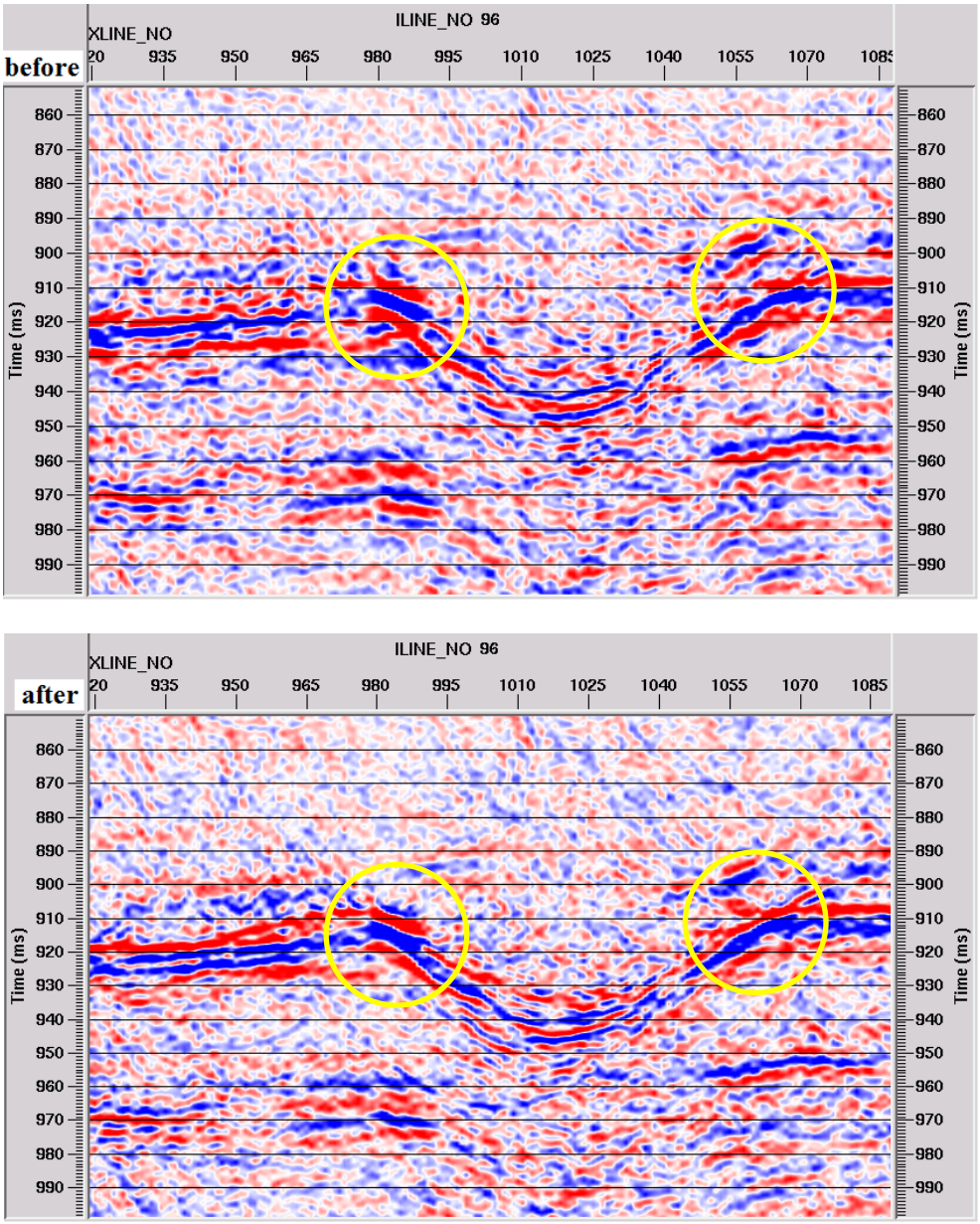

Figure 5: correlation match filters applied to the Snøhvit 2013 dataset.

The differencing phase of the 4D processing implies:

- computing variance, correlation or semblance between datasets;
- calculating and applying match filters;
- generating comparison displays.

The final product is a time-lapse difference volume obtained by subtracting one 3D volume from another (figure 6). The difference should be close to zero except where changes have occurred.

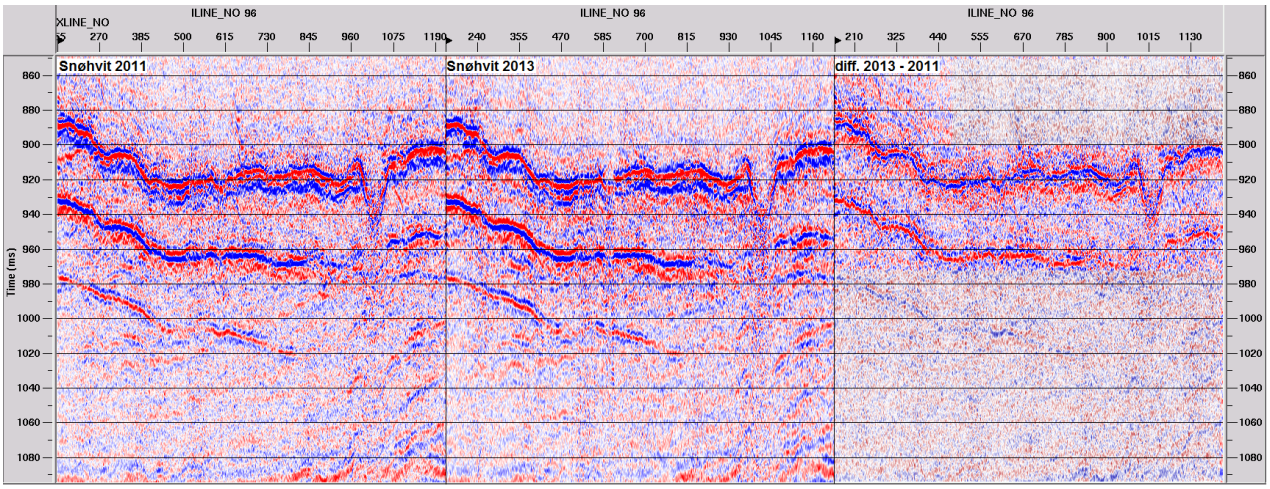

Figure 6: Snøhvit 2011 (left) & 2013 (centre) original cubes, final difference cube (right)

NRMS and Predictability parameters were calculated during the 4D processing of the Snøhvit datasets and results are presented in table 2.

	initial values	end of 4D preprocessing	after global shift	after amplitude CE	final values
NRMS	179.2 %	141.5 %	117.3 %	110.2 %	103.7 %
PRED	13.8 %	27.4 %	32.1 %	38.8 %	40.6 %

Table 2: likeness parameters calculated at different stages of the 4D processing.

2.3 4D processing and analysis at Vestnesa Ridge

The Vestnesa Ridge is a large sediment drift deposits located on the West-Svalbard margin. Active and inactive chimney structures occur along the crest of the ridge and have been mapped using high resolution P-Cable 3D seismic data. These chimney structures indicate the presence of free gas, which is also supported by the occurrence of a BSR 200 ms (twt) bsf (beneath seafloor) (Buenz et al., 2012). The 3D seismic data also reveal that the seepage zones are closely related to faults and fractures that reflect the influence of nearby tectonic stress (Plaza-Faverola, et al., 2015).

The Vestnesa 4D was preprocessed in Landmark's SeisSpace to match the geometry of the survey. The 4D processing and analysis was then done using the window based software Pro4D from CGG Hampson-Russell. Pro4D management system helps us organize the seismic data and offer several tools for analyzing and interpreting the time-lapse data. Leading edge survey calibration tools enables us to match the different 3D datasets in regards of frequency, phase, amplitude and event times of base and monitor in areas where fluid flow has not occurred. When the non-production induced variations have been removed the changes due to fluid flow can be analyzed. The software also offers a wide range of time-

lapse attributes that highlight production related anomalies. In the Vestnesa Ridge area several heterogeneities are detected, pockmarks and chimneys are the most apparent. These heterogeneities will contribute to the non-repeatability of the data sets.

The initial data sets and difference between the data sets is shown in Figure 7 and 8. The difference seismic image which is a subtraction of the base and monitor data show show large discrepancies which are mostly due to the non-matching phase of both data sets. However, the frequency spectrum in Figure 8 shows that both data sets contain the same bandwidth and amplitude distribution of frequencies. Both surveys have a peak frequency at approximately 175 Hz. This high frequency leads to a good vertical resolution, meaning that small vertical changes in the subsurface may be well mapped in the seismic data. Small changes due to fluid flow between base and monitor can then be detected in the time-lapse difference seismic.

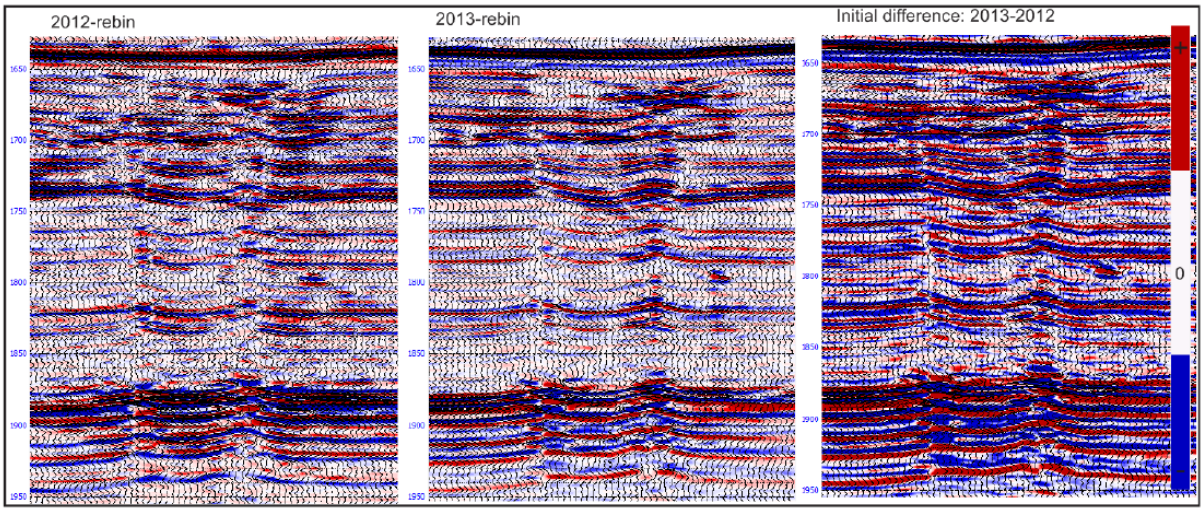

Figure 7: Seismic section showing base, monitor and the initial difference between the base (2012) and monitor (2013) surveys.

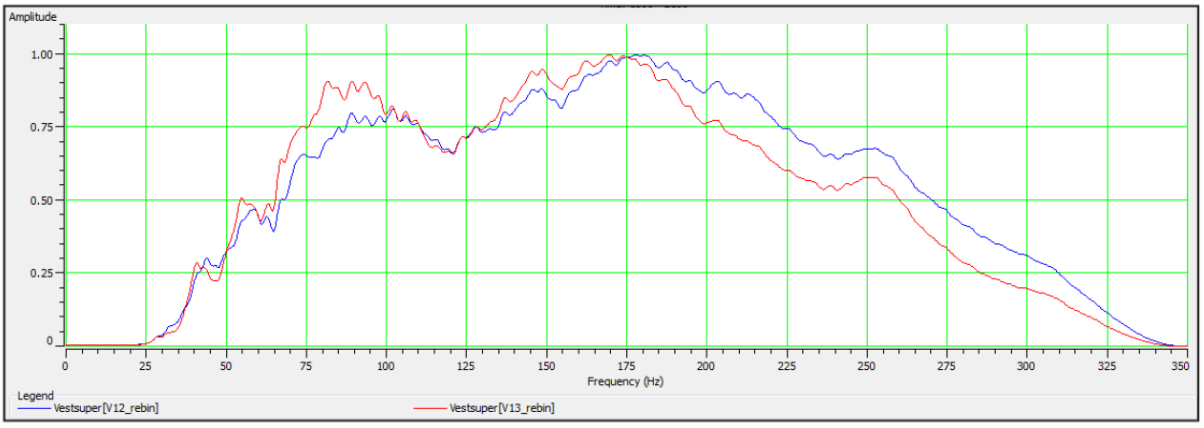

Figure 8: Amplitude spectrum, comparing frequency distribution between base (2012) and monitor (2013) survey, initial state.

2.3.1 Cross-correlation coefficients and time-shifts

Both cross-correlation coefficient and time-shift plots are a good way to highlight the difference between the two datasets. Correlation coefficients are a tool to help determine threshold parameters to use for calibration. One can compare the base and the monitor in regards of phase, frequency and time of events to estimate the common signals between traces. This will help when deciding which areas that have been affected by fluid flow in the subsurface, and hence which areas to avoid when correcting the "dead-areas"/making the signals in the two set as similar as possible.

The correlation slices created in this step (Figure 9) will help decide which areas to leave out of the processing window during data matching. In areas where the correlation coefficients are very low are expected to be due to fluid flow, and hence is being excluded in the calibration of the processing step, phase- and time-shift. The red areas in Figure 9 represent lower correlation (lower than 50%). In these areas the subsurface most likely has been affected be fluid flow within the gas chimneys and we want to leave these areas out of the processing calibration during data matching to avoid that the affected areas are being artificially reduced.

The mean correlation value is 48%, meaning that most of the area is affected by the degrading effect that heterogeneities, such as gas chimneys, has on seismic reflections. Since the chimneys are stretching in vertical direction it is impossible to pick a correlation window that will not be affected by these structures and the fluid flow within them, hence we need to use cross-correlation and time-shift threshold to calibrate the adjustments of the data in the following processing steps.

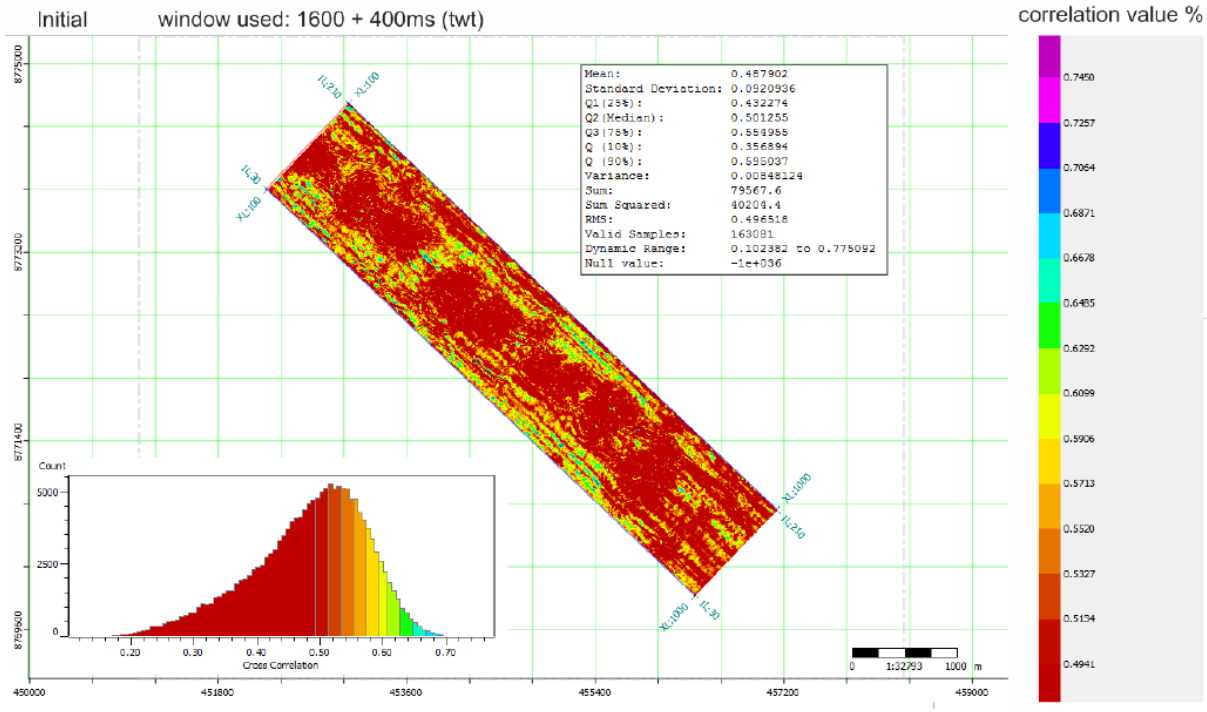

Figure 9: Base map of the 4D survey with cross-correlation values between the two datasets. Statics and histogram distribution of cross-correlation values also displayed.

The correlation time-shift slice (Figure 10) show the average bulk shift of time between the two datasets. The red values mean that the monitor survey (2013) is placed beneath base survey in ms (twt) (2012) in that specific area and the blue values mean that monitor survey is placed above base survey in ms (twt) in that specific area, since we subtract monitor (2013) from base (2012). The white values at zero mean that base and monitor is placed at similar depth in ms (two way travel time).

There is an average bulk time-shift of 1.34 milliseconds between the two datasets. This is not a major shift, but it can still lead to poor repeatability between the two sets. The striping effect on the plot most likely occurs due to acquisition and will be removed further in the processing flow.

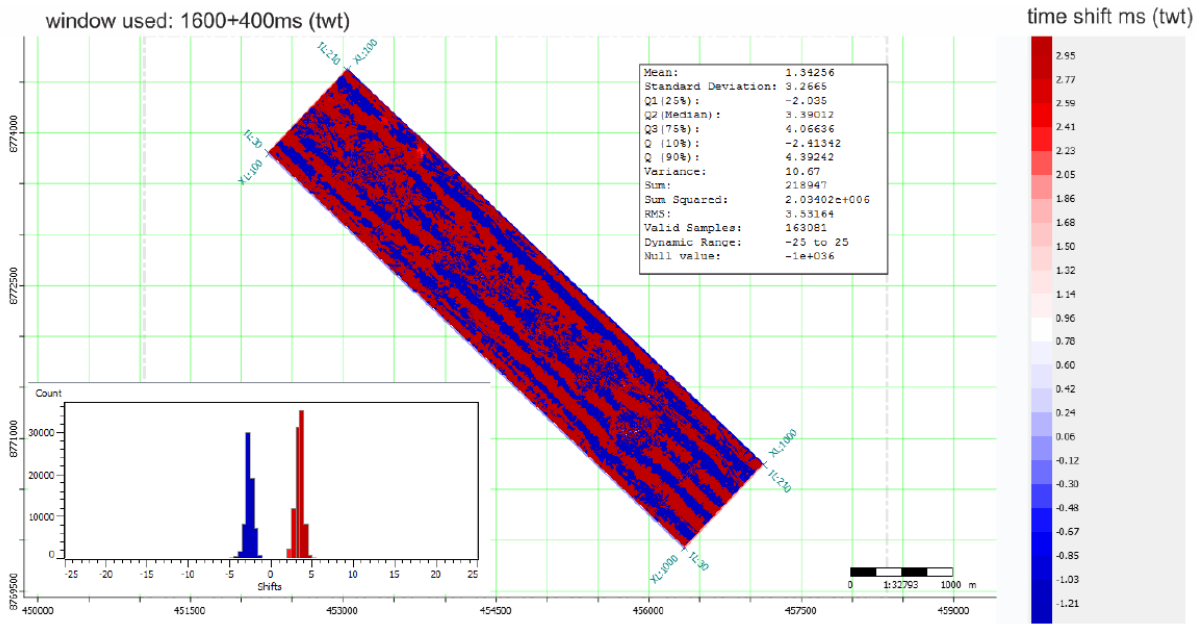

Figure 10: Time-shift plot, Initial state. Statics and time-shift histogram distribution also displayed.

2.3.2 Predictability between the two volumes

Predictability is a measure of how closely the two volumes values follow each other (Figure 11) or how similar they are. The statics from the maps created in this step will tell us the trends in matching between the two volumes. A good match would be close to 100%. In areas where there have been movement of fluid the predictability is often poor and we need to correct for this by calibrate the phase- and time-shift needed to match these two datasets.

If predictability equals 1 this means that the traces are perfectly correlated. The predictability is more sensitive to noise and distortion than to time shift. So even if the time shift is big, the predictability can still be good.

The average predictability value is 69, 31%, so the trend of the two volumes are not very close to each other. The areas where Predictability is lower than 60%, dark green color, have sub-circular shapes and vary in size, likely where the gas chimneys are located, and fluid flow has occurred.

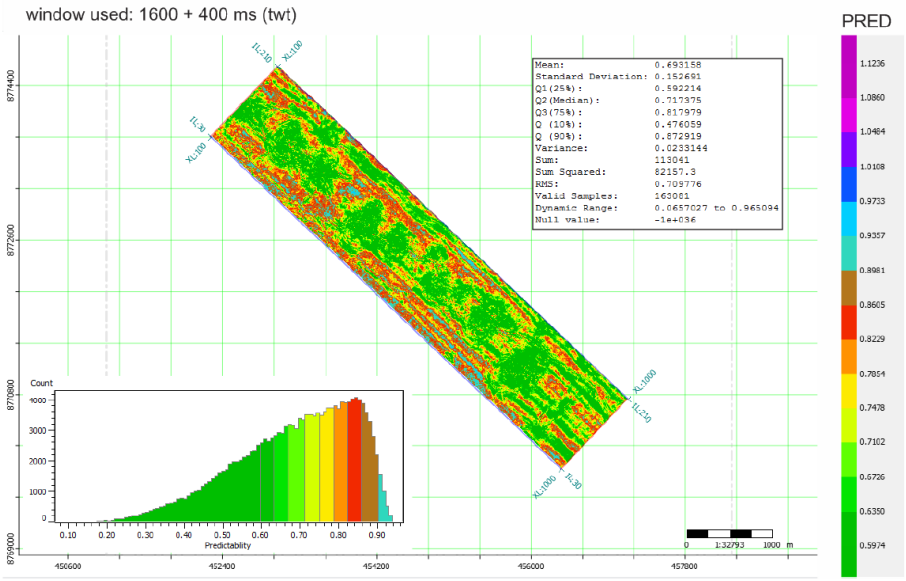

Figure 11: Predictability map, Initial state. Statics and histogram distribution of PRED also displayed.

2.3.3 4D processing

The first 4D processing step corrected for phase and time shifts described above. When applying the time- and phase-shift we set cross-correlation and time-shift thresholds at values in which only the traces that are equal or exceed these values are being used in the calibration process of the phase- and time-shifts. This ensures that the shift is being done only based on areas that correlate well and have not been affected by fluid flow. These corrections/shifts will be applied to the entire monitor volume. Global average is being used instead of trace by trace to preserve the trace variation in the data. Individual trace-by-trace corrections will be implemented at a later stage.

Only 16 081 traces out of a total of 163 081 passed the threshold, this means that a big percentage of the area in the two data sets have initial poor correlation to each other. A global time shift applied of 0.23 ms and a global phase shift applied of 106.012.01 degrees was applied. This gave a significant improvement in the difference volume (Figure 12). Several of the most apparent reflections are gone and less visible, but still there is considerable energy that most likely does not originate from changes due to fluid flow.

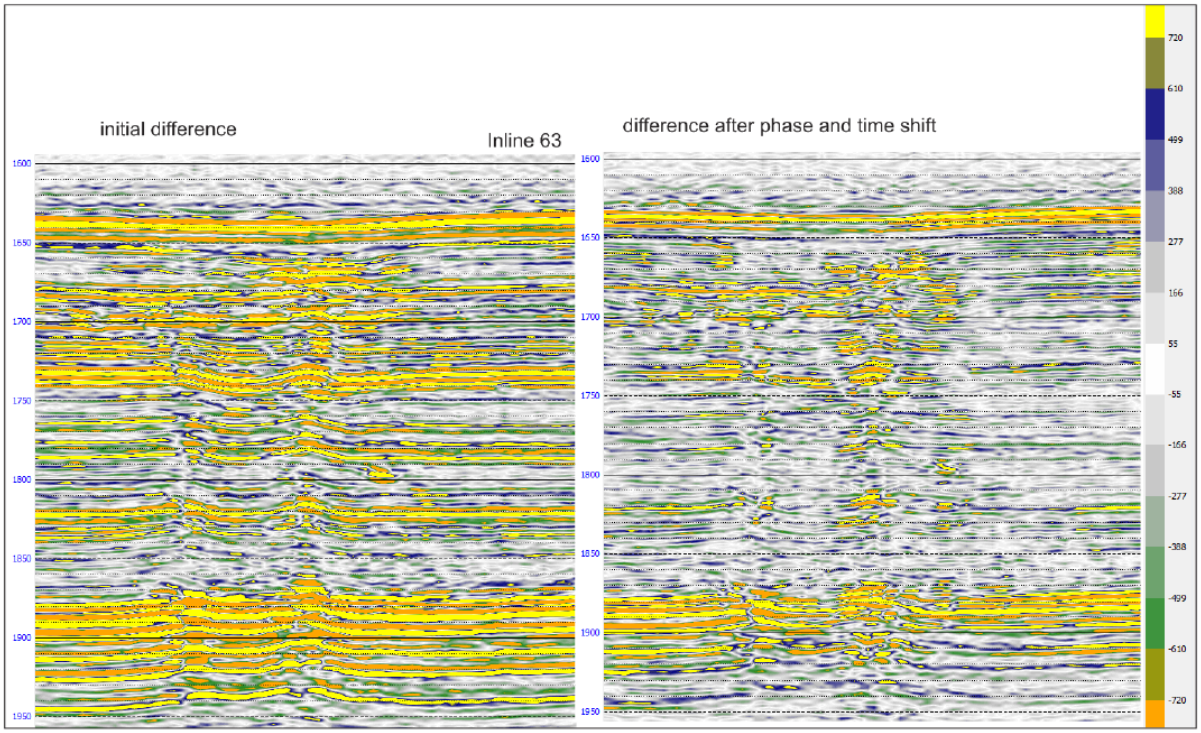

Figure 12 Seismic section showing initial difference and after phase- & time-shift was applied.

The next step applies a shaping filter in order to match frequency content, phase, time and amplitude of the two datasets. The zones that do not match well between the two volumes are being excluded from the filter calibration.

After the phase matching and prior to the shaping filter there were 105 712 traces out of 163 081 that passed the threshold, and the max correlation coefficient found was at 92.88%. During the shaping process there were 127 063 traces that passed the threshold, 22 000 more traces than during the previous stage, and the max correlation is now found to be 96.05%, this is a significant improvement. Several reflections have become less evident, especially in the top and bottom region of the seismic (Figure 13).

A better indicator, than the cross-correlation value, is the NRMS value between the two volumes (Figure 14).This calculates the overall similarities between the two data sets. The NRMS value has decreased from an average of 1.65 to 0.85, this is a decrease of 47% in NRMS from the initial state to after the phase- & time-shift and shaping filter process was applied. In general the present NRMS is still considered too high and further processing is needed.

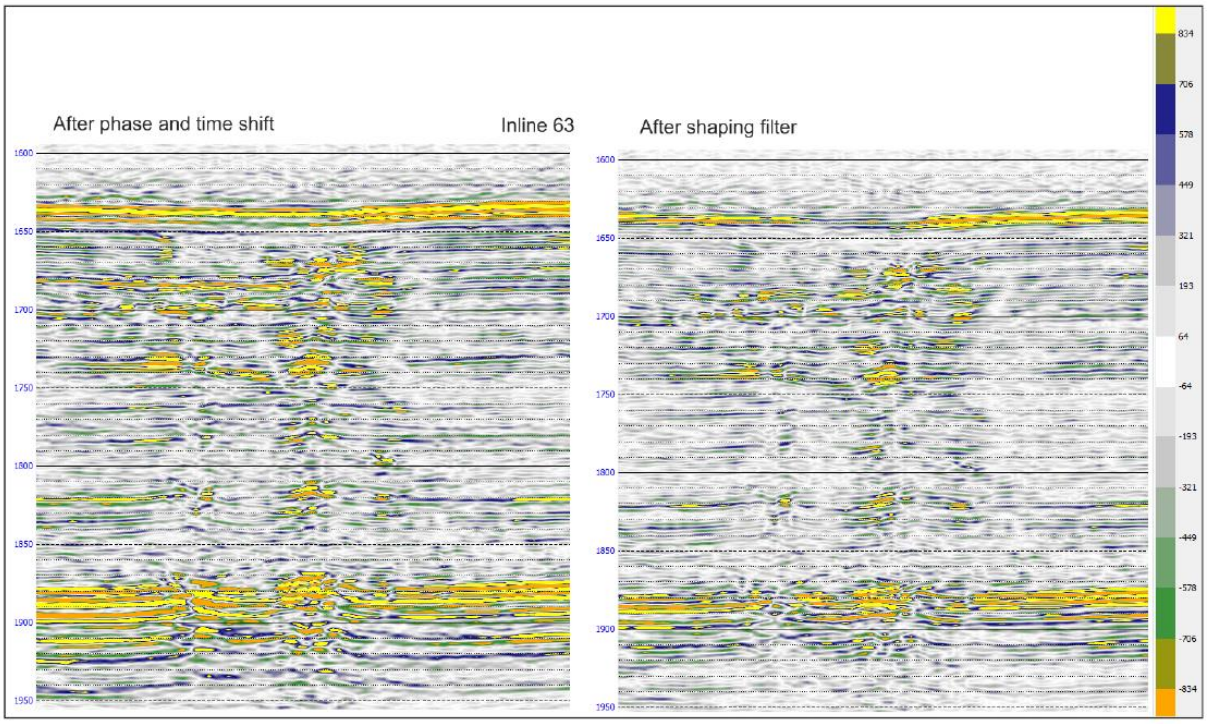

Figure 13: Seismic sections after phase- & time-shift and after shaping filter.

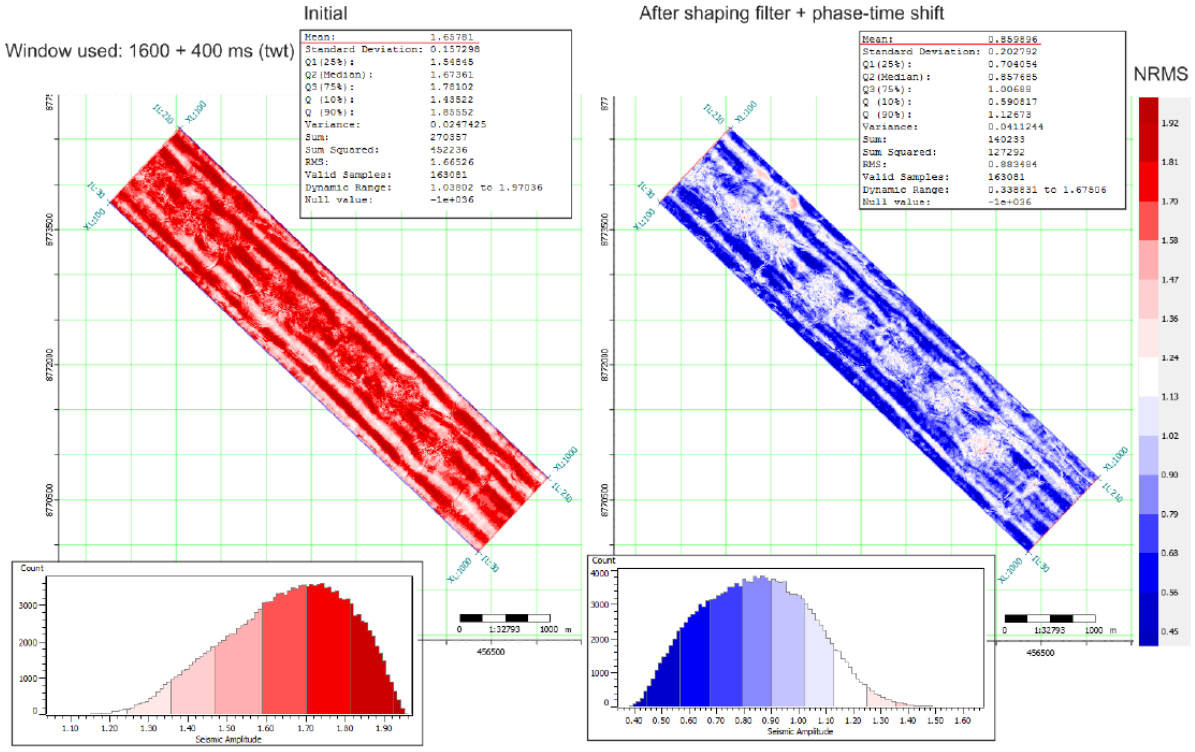

Figure 14 NRMS maps: initial & after phase & time and shaping filter was applied

The next step calculates the average amplitude difference between the volumes and provides and RMS scaling factor for the monitor volume to match amplitude levels. This step slight improved the NRMS between the volumes down to 0.84.

Velocity changes due to present of fluid/gas will affect the travel time of nearby events. By calculating the time-variant shifts we calibrate the adjustment needed to compensate for this. The most deviation from mean values in regards of time-shift and cross-correlation is found in areas where interpreted gas chimneys are detected on the seismic image.

By applying the time-variant shift the events in the monitor survey are now put in proper time in relation to base survey. The seismic difference between the two volumes has decreased significantly (Figure 15). Almost all of the most apparent reflections disappeared. Remaining amplitudes on the difference volume are located in a vertical zone around the locations of an interpreted gas chimneys.

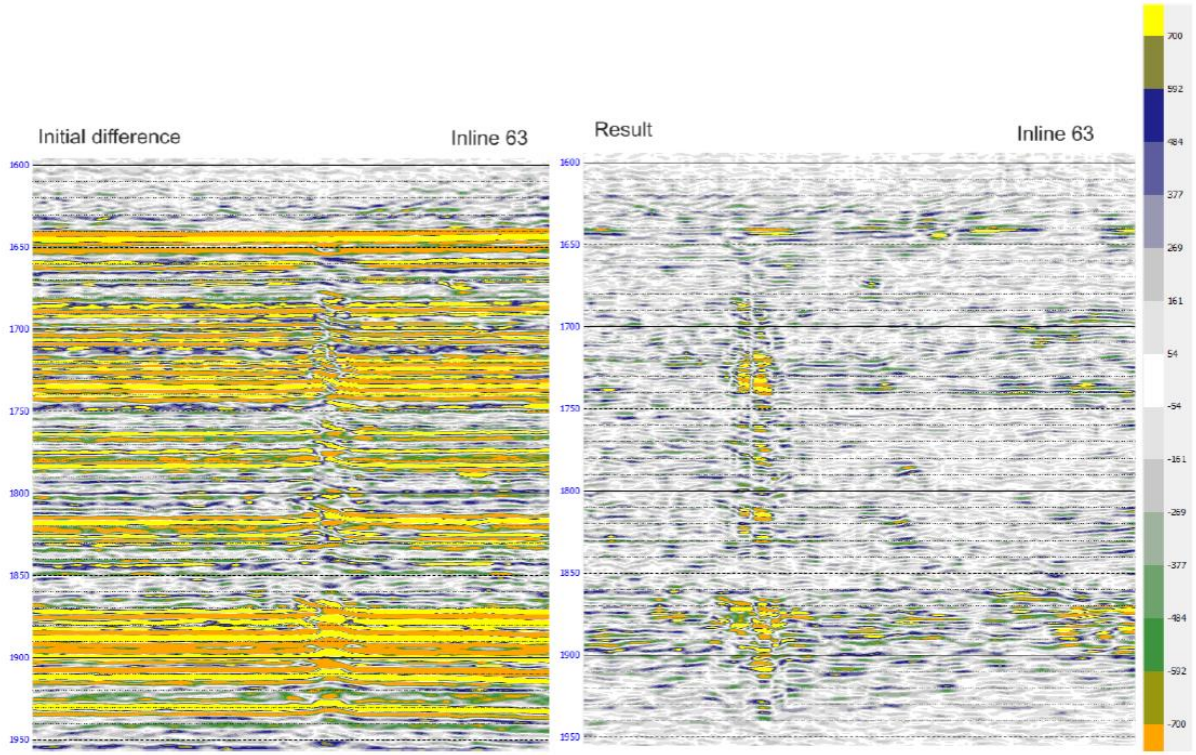

Figure 15: Seismic sections: Initial difference & difference after full 4D processing flow applied.

The mean cross-correlation value after the final step of processing is 0.79, this is significantly higher than before any processing had been done on the data with a mean cross-correlation value of 0.48 (Figure 16). The area with lower predictability, green color (Figure 17), have sub-circular shapes and are likely to lie within the areas that correspond with the locations of several gas chimneys. The mean predictability between the two data sets is now 0.75, this is an improvement of 0.06 since before any processing had been done. However, most of the data outside of the chimneys have high predictability of better than 80%.

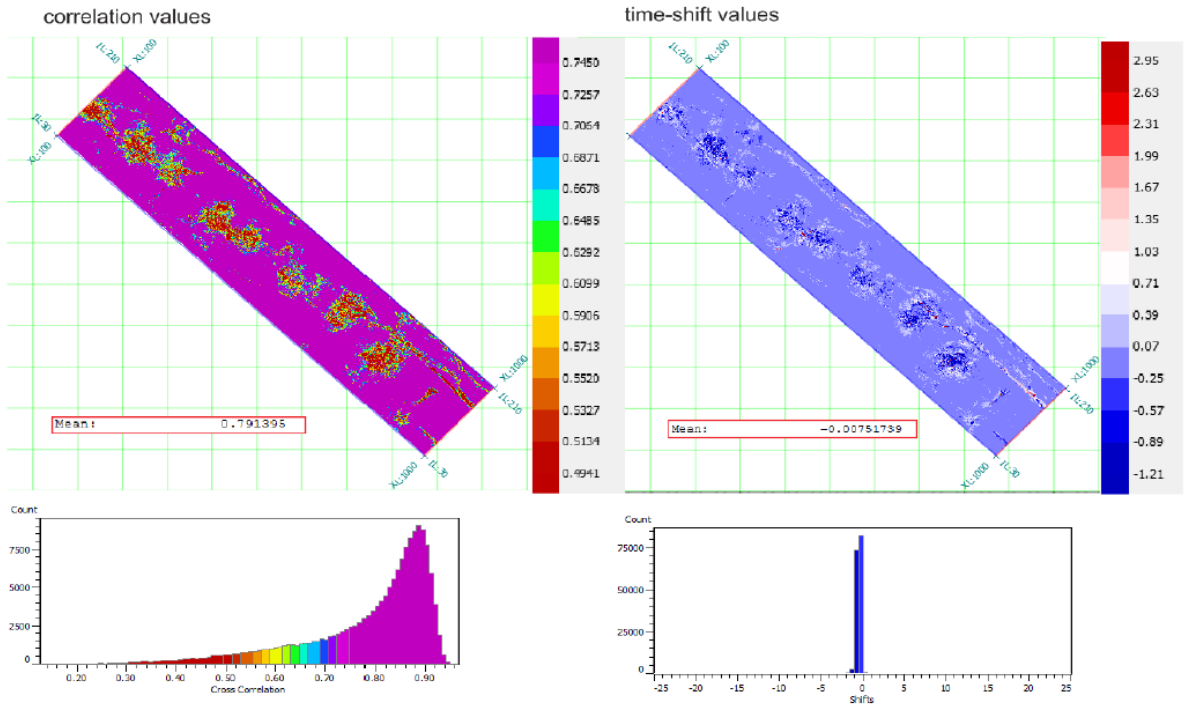

Figure 16 final cross-correlation and time-shift values. Window used: 1600 + 350 ms (twt).

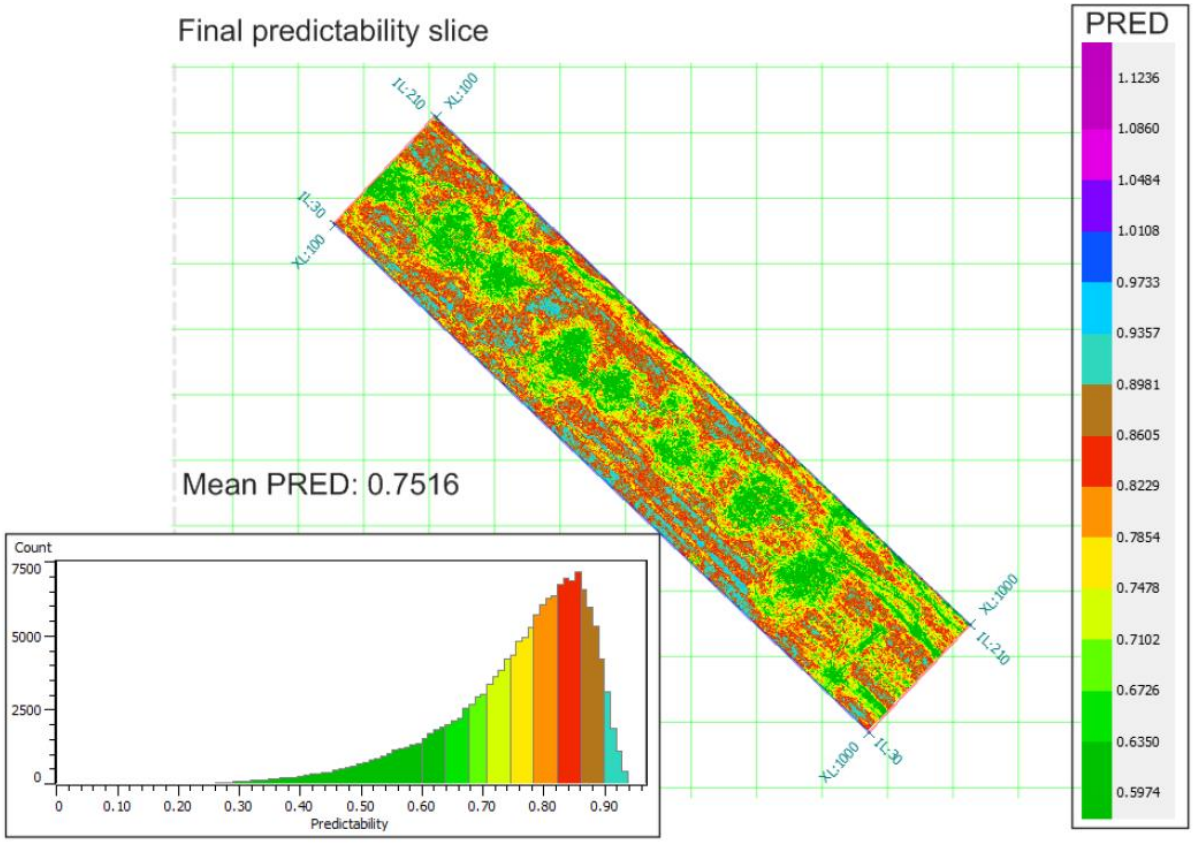

Figure 17: final predictability slice. Window used: 1600 + 350 ms (twt)

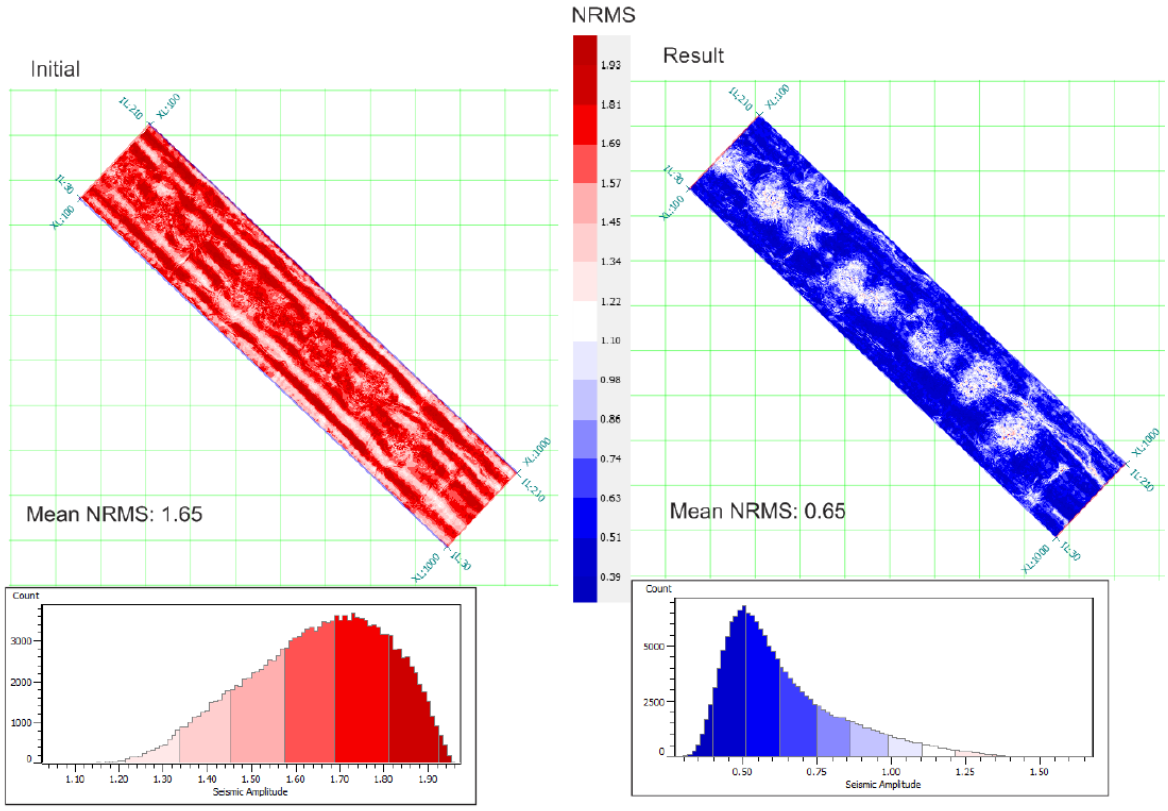

Figure 18: NRMS plot of initial unprocessed volumes and after 4D processing, respectively.

The NRMS values have decreased from a mean of 1.65 to a mean of 0.65, this is an improvement of 60 % from initial to final result (Figure 18). The acquisition footprint, striping effect, on the NRMS slice is gone and the areas where one expects the location of gas chimneys are quite apparent on the final slice. The sub-circular white areas have the highest NRMS values at the final slice, as expected. In these areas, where the interpreted gas chimneys occur, are expected to have changed the most between the two surveys, since leakage of gas through these structures likely has occurred.

2.4 Concluding remarks on the 4D seismic processing of P-Cable 3D seismic data

The main focus of this subtask was to develop the P-Cable 3D seismic technology into a monitoring tool for the shallow subsurface. The frequency bandwidth is much wider and the high frequencies are very sensitive to small changes in the subsurface. By use of high frequency P-Cable data one may not expect the same matching results with regards to 4D attributes (NRMS, predictability and correlation) as obtained from 4D processing of conventional seismic data. However, the 4D processing sequence developed here is promising and can be further developed by application in other areas and by improvements in the

original 3D seismic processing, implementing trace-by-trace analysis, analysis of sub-domains of the data and application in other areas that are less affected by fluid flow features.

3 Testing leakage detection thresholds using high frequency p-cable seismic data

3.1 Introduction

The primary tool for determining the distribution of CO_2 in the subsurface following injection is 4D seismic. The methodology makes use of the fact that small amounts of CO_2 can produce detectable difference signal during time-lapse seismic analysis (Figure 19).

However, the costs of full 3D seismic surveys mean the intervals between surveys can be significant. One additional problem with conventional seismic acquisition is the lack of focus on the overburden, especially the zone close to the seabed, where the fold of cover is reduced and the velocity analysis during processing is sometimes neglected.

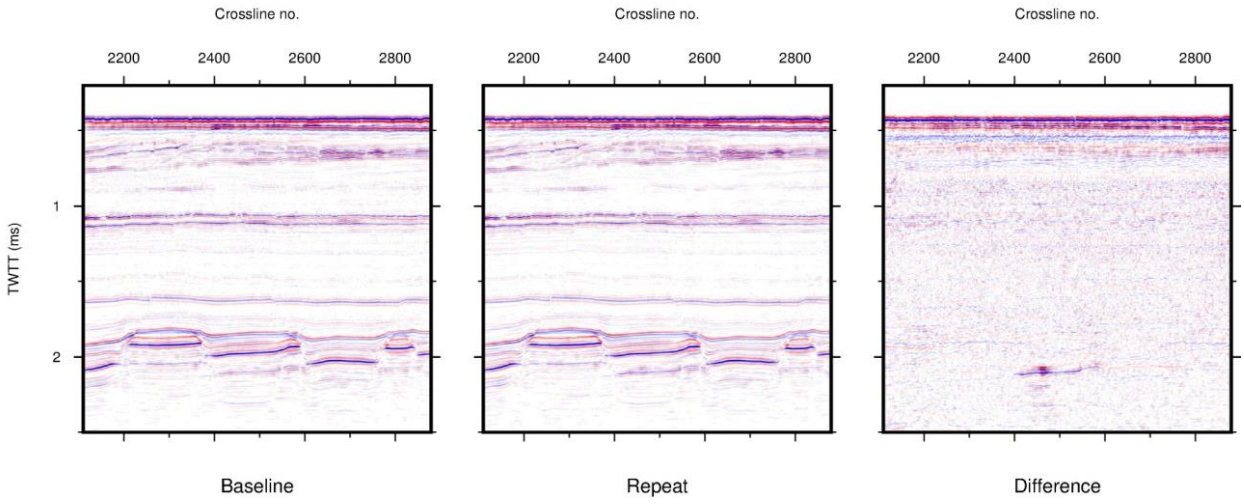

Figure 19. Conventional 3D seismic data from the Snohvit CO_2 injection site. Detection of a CO2 anomaly is difficult using only the baseline (2003) and repeat (2009) surveys, but the difference data clearly shows the effect of CO2 injection. The uppermost response in the difference section comprises both a saturation and pressure effect whilst the underlying refecltions in the difference cube are a result of velocity pushdown.

CO_2 leaking from a storage complex will also produce a detectable signal on seismic data if a sufficient amount pools together. This threshold for detection is dependent on the volume of CO_2, the depth of accumulation and the signal to noise ratio of the data, which is optimised during the processing sequence. One option to image the near seabed is to use a cheaper, shorter offset, 3D seismic data acquisition strategy. One such system is the high resolution p-cable 3D seismic method. Using this approach, low-fold, high resolution seismic data is acquired with short streamers. As such, the system is well placed to image the top 500 m below the seabed.

Here, a novel quantitative approach, which determines the detection limits of small reflectivity changes as a function of both amplitude and spatial extent, is applied to the P-cable data. The detectability of small leaking CO_2 volumes in the overburden is tested with P-cable data. Parts of the overburden are quiet and would be expected to display high detection capability, whereas other parts are noisy and detection capability is likely to be reduced.

The University of Tromso have acquired two high resolution P-cable 3D seismic data surveys at the Snohvit Field, Barents Sea. These surveys acquired in 2011 and 2013 have the same footprint and cover an area of 8 x 2 km. Whilst these surveys do not overlap the conventional time-lapse seismic surveys (used to image the CO_2 injection operation) they are only offset by ~2 km. The p-cable data has been used to image shallow gas and gas hydrates and to map fluid migration pathways close to the sea floor. The original study aims for the data in the Snohvit region were to image pockmarks and shallow fluid pathways.

The high frequency content of the p-cable data (50 - 300 Hz), and the optimised acquisition set-up ensures an improvement in temporal and spatial resolution over conventional 3D seismic data.

3.2 Potential CO_2 leakage

The CO_2 injection operation at Snohvit provides an excellent location to test the novel spatial-spectral detection methodology discussed in this study. Here, both conventional 3D seismic and 3D p-cable data are available in the same tectonic setting.

CO_2 Injection commenced in April 2008 with the initial phase of injection at the base of the Tubaen Formation. This fluvial to tidal sandstone deposit is approximately 100 m thick, at 2565-2665 m depth below sea surface. Injection into the Tubaen was abandoned in 2011 due to unexpected pressure increases. This was followed by a further phase of injection, utilising the same well, into the overlying Sto Formation. This injection continues today, without any observed pressure increase. No leakage of CO_2 has been identified during either phase of injection. However, this study postulates the effect of a CO_2 leak into the overburden and determines the probability of detection following such a scenario.

Within the overburden, at depths shallower than the storage reservoir, the CO_2 will become less dense as it moves towards the seabed. It is expected to develop greater reflectivity, and accordingly greater detectability as it moves from a dense phase to a gaseous one. This work fits neatly with the European CO_2 storage directive where a site operator is required to demonstrate zero detectable leakage in order to transfer responsibility to national authorities. Within this scope, leakage would be defined as a CO_2 escape from the storage complex, the top of which would likely be defined at a level in the overburden. As such, studies such as this which define detection thresholds will play an important role in determining the volumes of CO_2 that may leak unnoticed.

Leaking CO_2 is likely to accumulate as either thin sub-horizontal cones/layers or vertical chimneys, which preferentially occupy zones of higher permeability. The difference signal generated by the CO_2 will be evident either as a reflection from the CO_2 itself, or by the pushdown of deeper reflections generated as a consequence of the velocity reduction brought

about by fluid substitution. To demonstrate this, Figure 20 uses the log data from well 71206-1 at Snohvit to generate a 2D velocity model of the subsurface in the region. Synthetic seismic data for the baseline case was generated using a phase screen forward modelling code (White and Hobbs, 2007).

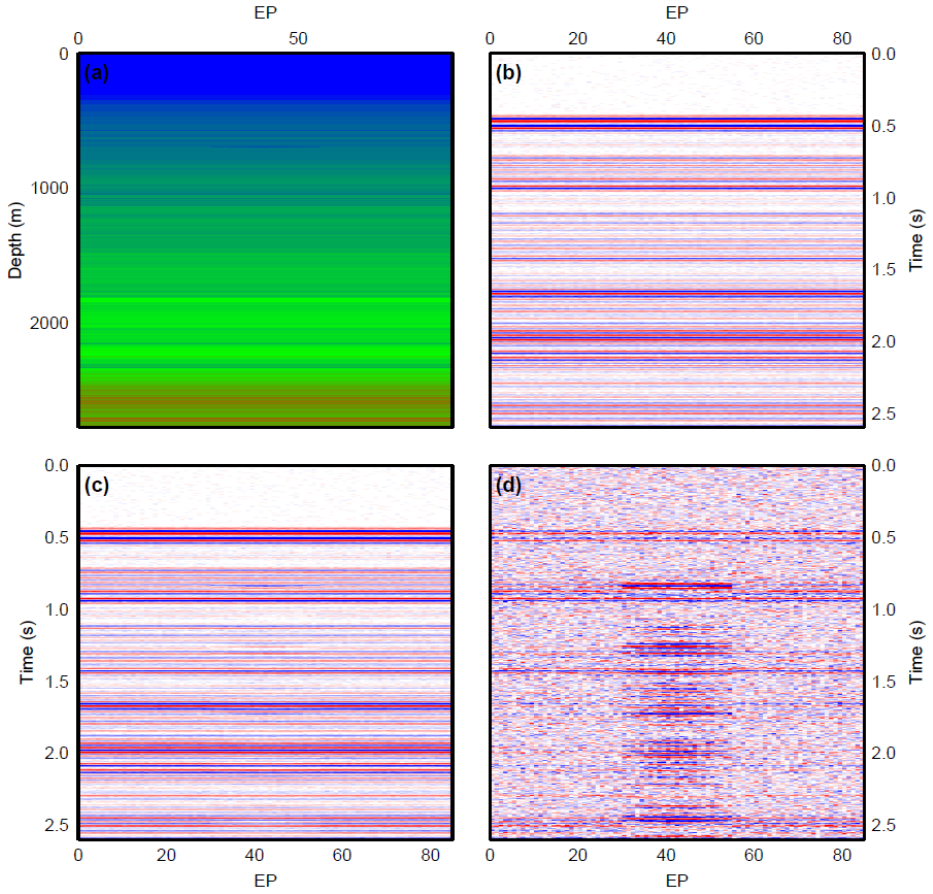

Figure 20. CO_2 leak at 700 m, saturation=0.8. (a) Velocity model; (b) baseline survey; (c) repeat survey; and (d) difference section.

Noise levels were determined using two techniques, both utilising the time-lapse seismic data. Firstly, random noise was derived by comparing the spectral characteristics of a traces mean auto correlation with the cross correlation of a trace and its neighbour. The difference between the two was judged to contain the random noise. Additionally, a systematic noise component was added by calculating the total windowed RMS amplitude along each time-lapse difference trace. The noise was then added to the synthetic data and NRMS and predictability compared favourably with the time-lapse seismic suggesting the approach was reasonable. Small CO_2 leak could then be added to the model.

Mineral content control was limited in the overburden and generic shale parameters are used to determine bulk moduli for this region. Span and Wagner's equation of state for CO_2 is used to derive the correct gas properties as a function of pressure and temperature and

Gassmann fluid substitution equations were used. Figure 3 shows an example of the response for a cone of maximum thickness 4 m. The reflection from the CO_2 is evident but the primary response (for this high saturation, higher porosity example) is the noticeable pushdown throughout the section.

3.3 P-cable data

The p-cable data were acquired to the south of the Snohvit field with a water depth of ~300 m. The region is characterised by E-W trending faults and significant uplift. The major tectonic activity is Upper Jurassic-Lower Cretaceous in age (Dore, 1995). Figure 21 shows the same section for the 2011 (left) and 2013 (right) p-cable surveys.

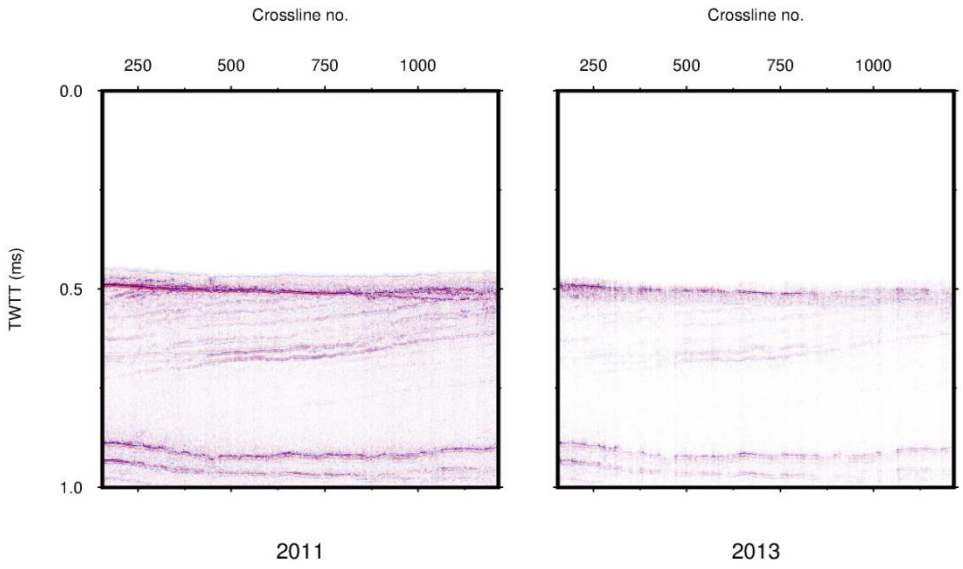

Figure 21. Equivalent in-line sections from 2011 and 2013 p-cable 3D seismic data sets.

It is apparent that the sea-bed reflection has been removed during processing. The sub-horizontal reflection beneath the seabed images the Upper Regional Unconformity (URU) which separates the overlying glacial deposits from the dipping layers of the Torsk Formation. Additionally it is clear that the sea-bed multiple has not been removed during the processing. Upon reviewing the data, near sea-bed bright spots, high amplitude anomalies and a series of well imaged clinoforms are revealed.

However, the problems with the time lapse processing are clear from studying the different vintages, as reflection amplitudes do not appear to be consistent. Figure 22 shows the same inline (168) as Figure 4, but from the seismic difference cube (2013-2011). Here the remaining signal can be considered as noise but it is clear that its nature is not random. Signal relating to geological interfaces dominate the response, clearly demonstrating the further time-lapse processing is necessary to improve the differencing.

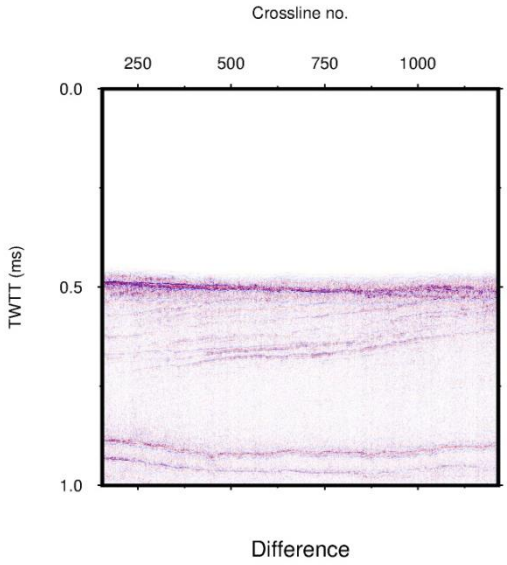

Figure 22. High resolution p-cable seismic difference data from inline 168.

Due to the current state of the time-lapse processing, the methodology described in the study will produce results that are not optimal. A more robust processing scheme would ensure significant improvement in the detection thresholds, especially in the regions where the geological interfaces are imaged.

3.4 Methodology - Statistical analysis

The statistical analysis undertaken in this study necessitates the selection of time-slices, or picked surfaces, from the p-cable 3D seismic difference cube. Figure 23 illustrates the location of time-slices at 510, 560, 610 and 660 ms.

Amplitudes grids are exported from 3D p-cable seismic difference data for each of the surfaces (Figure 24). These amplitude slices are considered to display repeatability noise but some show significant geological signal that has been poorly matched in the time-lapse processing. The grids are considered to represent the noise between different the time-lapse vintages. It is clear that further time-lapse processing would improve this response significantly.

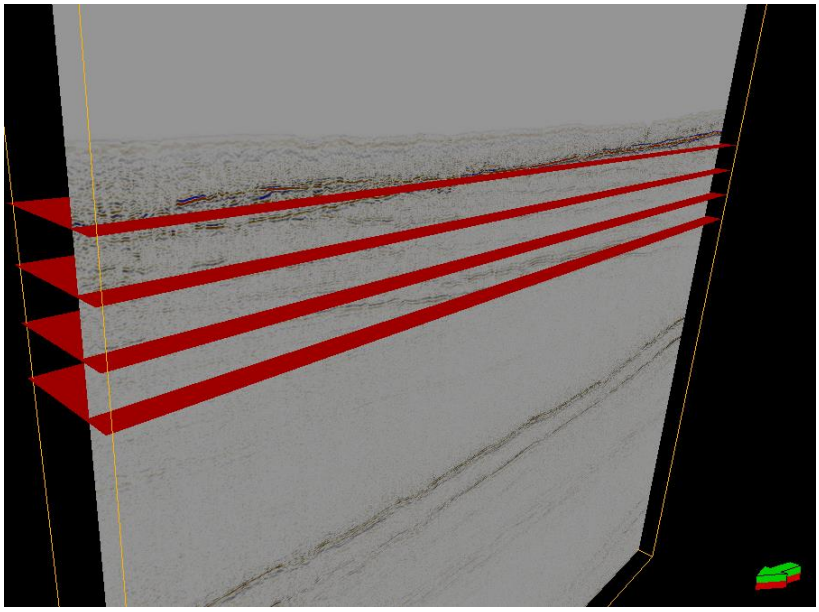

Figure 23. The extraction of time-slices from the high resolution p-cable seismic difference data.

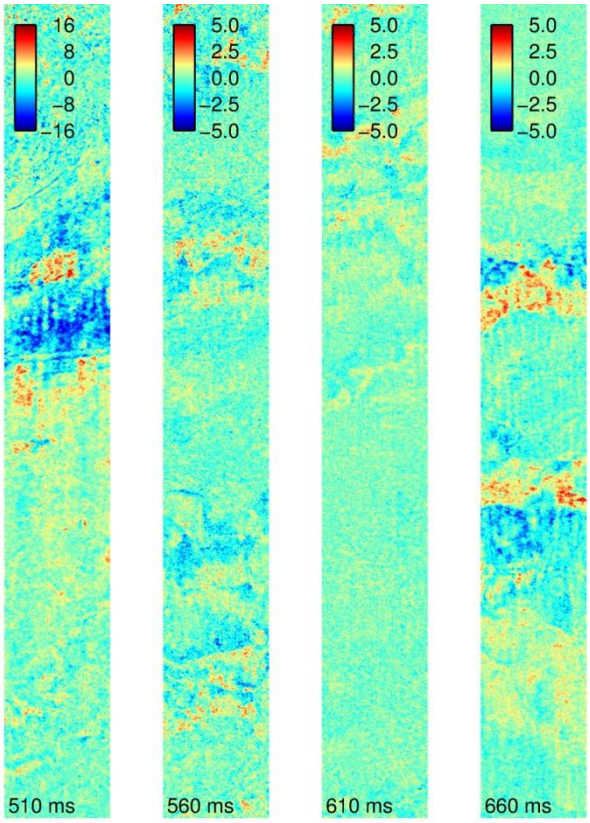

Figure 24. Amplitudes extracted from p-cable seismic difference data cube at constant times (510, 560, 610 and 660 ms). Note: the scale on the 510 ms grid is different to the others as this section intersects the reflection from the URU.

The discrete wavelet transform is used to decompose the noise on the time-slices extracted from the overburden. The grids are decomposed into a series of components which each represent a different spatial scale length. Each component represents the noise level for that time-slice over the defined scale length. Once the noise levels have been assessed, it is possible to use the approach to discriminate the noise from leaking CO_2. If a single component shows a clear increase above the noise in subsequent vintages, then this change would be highlighted. The threshold is set at 1.5 times the coefficient determined at each scale.

A set of tests was carried out to examine the detectability of synthetic CO_2 accumulations by adding circular reflections (amplitude anomalies) of known size and of uniform amplitude. The synthetic accumulations are added at random locations to the time-slices. By running the simulation many 1000's of times we can produce statistical likelihoods of detection as a function of amplitude and area. The area is defined in terms of number of bins – with bin size 6.25 x 6.25 m. Figure 25 displays the probability of detection and it is clear, in all cases, that this increases with area and reflectivity amplitude.

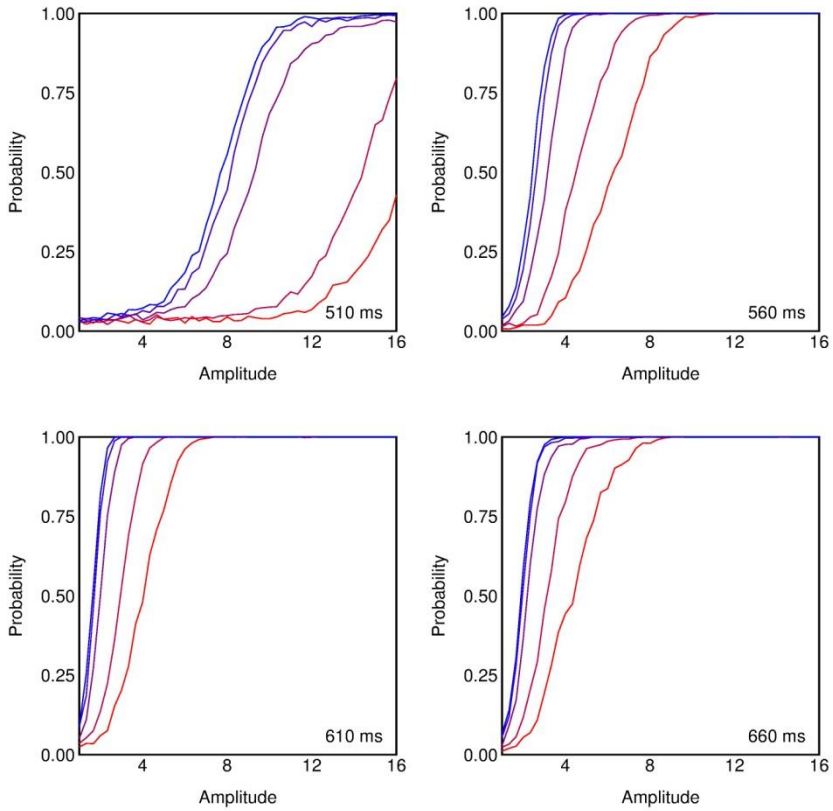

Figure 25: Probability of detecting synthetic features (leaks) with the overburden at 510, 560, 610 and 660 ms. The lines, from red to blue respectively, represent accumulation areas of 1, 5, 21, 45, and 69 bins.

It is clear that detectability is heavily influenced by the remnant signal in the time-lapse data. The noisy zone at 510 ms has comfortably the lowest probability of detection. Ordinarily, it would be expected that depth would be the primary influence on the detectability of leakage.

So far, this study has classified detectability as a function of reflection amplitude. This can be scaled to layer thickness, for thickness beneath the tuning thickness, if the properties of the subsurface are known. This approach requires a reflection in the seismic section where the acoustic impedance contrast is known. This result can then be use to scale the reflections from a CO_2 layer. Unfortunately, the seabed reflection has been muted in this data set. As such focus turned to the URU reflection. Regional data suggested a velocity increase at this interface from 1500 to 1850 (Tasianas, pers comm.). Synthetic seismic modelling, with a velocity model replicating the water column, glacial sediments and the Torsk Formation was undertaken. CO_2 was added to the model as a thinning layer. Figure 26 shows the synthetic response.

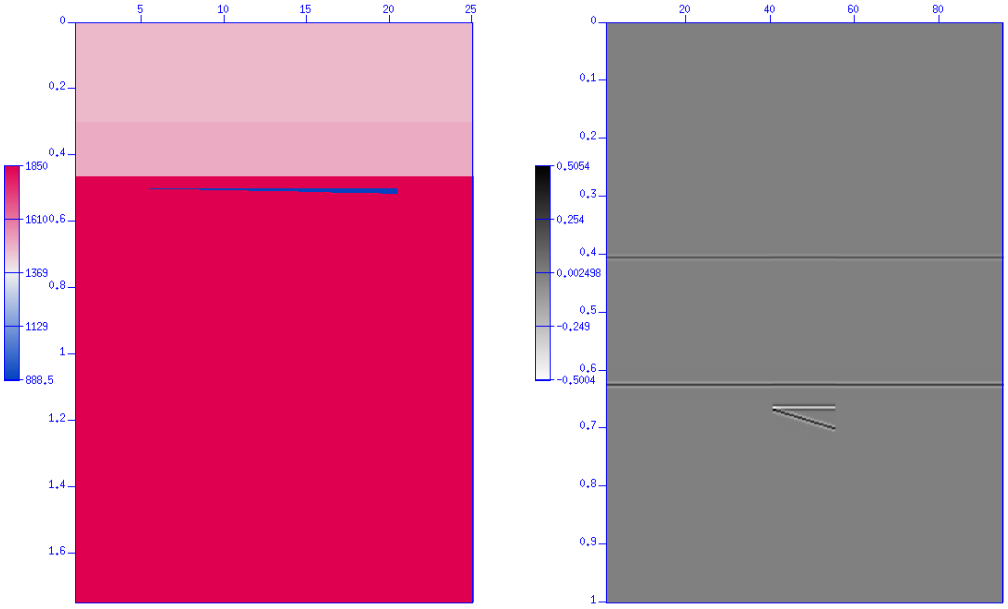

Figure26. Left - Simple velocity model of seabed and URU with thinning CO_2 layer added. Right - The seismic response.

Unfortunately the difference in amplitude of the URU reflection between the two time-lapse vintages (Figure 23) prohibited the scaling of amplitude to thickness.

3.5 Concluding remarks on the estimation of detection thresholds from P-Cable 3D seismicdata

A methodology to determine the detectability of small amounts of leaking CO_2 has been tested on time-lapse high resolution p-cable data. The technique uses time-slices from the difference data and decomposes the grids into a series of components which each represent a

different spatial scale length. Amplitude anomalies, which represent CO_2 accumulations, are then added to the grids and the statistical likelihood of detection is determined as a function of amplitude and area. It is not possible to define a single detection threshold for a complete dataset. The limits of detection vary with depth and signal strength. However, these studies should lead to an approach which defines the optimal monitoring horizons in the overburden. Monitoring for CO_2 in the shallow overburden has several advantages. At shallower depths the decreasing density of CO_2 also contributes to improving detectability. Reflection amplitudes are greater and less mass of CO_2 is required for equivalent volumes.

Further work using picked surface, rather than constant time-slices, where leaking CO_2 leak may be more likely to pool, is currently underway.

It is hoped that the further development of this methodology, alongside a significant improvement in the time-lapse processing will enable a study comparing the relative detectabilty of leaking CO_2 with conventional and p-cable seismic data.

4 References

Buenz, S., Polyanov, S., Vadakkepuliyambatta, S., Consolaro, C., & Mienert, J. (2012). Active gas venting through hydrate-bearing sediments on the Vestnesa Ridge, offshore W-Svalbard. Marine Geology, v. 332, p. 189-197.

Eriksrud, M. (2014). Seabed permanent reservoir monitoring (PRM) -A valid 4D seismic technology for fields in the Nort Sea. EAGE.

Johnson, D. H. (2013). Practical Application of Time-lapse seismic Data . Tulsa, USA : Society of Exploratin Geophysicists .

Oghenekohwo, F., & Herrmann, F. (2013). Assesing the need for repeatability in aquisition of time-lapse data. 1-5.

Petersen, C. J., Büenz, S., Hustoft, S., Mienert, J., & Klaeschen, D. (2010). High-resolution P-cable 3D seismic imaging of gas chimney structures in gas hydrates sediments of an Arctic sediment drift. Marine and Petroleum Geology, vol. 27, pp. 1981-1994.

Plaza-Faverola, A., Buenz, S., Johnson, J., Chand, S., Knies, J., Mienert, J., & Franek, P. (2015). Role of tectonic stress in seepage evolution along the gas hydrate-charged Vestnesa Ridge, Fram Strait. Geophysical Research Letters, 42(3), 733–742.